Journal of the Serbian Society for Computational Mechanics / Vol. 19 / No. 1, 2025 / pp 347-361 / review paper
(10.24874/jsscm.2025.19.01.21)

NUMERICAL SIMULATION OF AORTIC DISSECTION: EVALUATING VIRTUAL SURGICAL INTERVENTIONS FOR IMPROVED HEMODYNAMIC OUTCOMES AND PERSONALIZED TREATMENT PLANNING

Igor Saveljic[1,3*] [0000-0002-0707-5174], Tijana Djukic[1,3] [0000-0002-9913-6527], Smiljana Tomasevic[2,3] [0000-0002-5614-5730] and Nenad Filipovic[2,3] [0000-0001-9964-5615]

[1] Institute for Information Technologies, University of Kragujevac, Kragujevac, Serbia, e-mail: isaveljic@kg.ac.rs
[2] Faculty of Engineering, University of Kragujevac, Kragujevac, Serbia
[3] BioIRC Bioengineering Research and Development Center, Kragujevac, Serbia
**corresponding author*

Abstract

Aortic dissection is a severe clinical condition that demands a thorough understanding of the interactions between the true and false lumens. In this study, numerical simulations were performed for two patients, generating two preoperative and two postoperative models. The analyses were carried out using the PAKSF solver, a specialized tool for fluid–structure interaction problems. The objective was to evaluate the influence of virtual surgical interventions by examining essential hemodynamic parameters, including shear stress, pressure, and flow velocity in both lumens. The findings indicate that virtual surgical modeling can serve as a valuable tool for surgical planning, providing improved insight into post-intervention hemodynamic alterations. Moreover, this methodology supports patient-specific treatment strategies, contributing to optimized outcomes. Overall, the results highlight the potential of numerical simulations in clinical practice, particularly for the management of complex vascular disorders..

Keywords: Aortic dissection, false lumen, numerical simulations, PAKSF solver, virtual surgical modeling

1. Introduction

Aortic dissection, sometimes referred to as a dissecting aneurysm of the aorta, involves a lengthwise split in the vessel wall that allows blood to flow into a new passage, forming an additional false channel. This process starts with a tear in the innermost layer (intima), enabling blood to seep into the vessel's inner structures. The tear is generally horizontal and does not circle the full circumference of the aorta (Khan et al. 2002).

The false channel is a blood-containing area located between the divided layers of the arterial wall. Based on the size of the tear, its enlargement can substantially squeeze the true

channel (Fig. 1). In the systolic phase, the true channel widens, while it narrows in diastole because of varying pressure. Blood in the true channel moves ahead during systole and tends to stay along the aorta's outer side. In the false channel, blood moves more slowly, and reverse flow can sometimes occur.

By evaluating the thickness of the wall and features of the initial tear, one can identify the beginning and end of the dissection. Dissections of the aorta are categorized as communicating or non-communicating based on blood flow patterns in the false channel. In communicating types, blood in the false channel can flow forward, backward, or with a delay. During the heart cycle, an acute dissection can lead to active movement of the intimal flap, and with restricted connection, clots may form. In non-communicating types, a clot occupies the false channel, blocking blood movement. This variant stems from a break in the middle layer, causing bleeding within the wall.

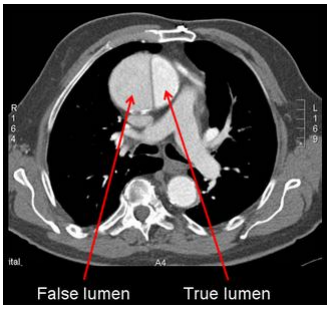

Fig. 1. Presence of false lumen

A range of direct and indirect, invasive and non-invasive imaging methods are utilized to diagnose aortic dissection. The main aim of these imaging approaches is to precisely detect whether an acute aortic dissection is present or not, categorize its type, locate the intimal tear, distinguish the true from the false channel, identify any clots, evaluate if aortic branches are affected, and spot any fluid leakage into the pericardium, mediastinum, or chest cavity.

Considering the critical role of precise diagnostics, the main aim in managing acute aortic dissection is to avert life-threatening events and permanent ischemic injury to the abdominal viscera and legs. In contrast to individuals with acute Type A dissection, who generally need operative repair, those with acute Type B dissection are often treated conservatively with drugs, assuming no major issues develop (Erbel et al. 2014; Isselbacher et al. 2022). Evidence from studies (Nienaber et al. 2016; Evangelista et al. 2018) backs this strategy due to:

- About two-thirds of the roughly 85% of individuals released from hospital after pharmacological management achieving favorable results without issues, thanks to intensive blood pressure control (Svensson et al. 2008).
- Minimizing hazards linked to urgent operations.
- Similar extended survival figures for medically and surgically managed cases. In every case of suspected acute aortic dissection, performing at least one imaging examination is vital to verify the condition, exclude alternatives, and choose the best therapeutic plan.

The key purpose of operative treatment for Type A (Types I and II) aortic dissection is to stop vessel rupture or fluid buildup in the pericardium, potentially causing tamponade and fatality. Moreover, abrupt aortic valve leakage and blockage of heart artery blood supply

demand immediate intervention. The objective involves substituting the affected area, defined by the inner layer split, using a synthetic conduit. Conversely, in acute Type B (Type III) aortic dissection, the focus is on avoiding vessel burst. Multiple management options are available, providing diverse technical possibilities (Culliford et al. 1982; Miller 1991; updated in Hiratzka et al. 2010).

2. Literarure review

Numerical simulations of blood flow dynamics in the aorta—considering both healthy cases and those affected by dissection—as well as analyses of flow and pressure within obstructed aortic branches caused by dissection, represent an important tool in modern medicine. Such simulations contribute significantly to understanding disease mechanisms and provide physicians with valuable support in clinical decision-making.

According to the International Registry of Acute Aortic Dissection (IRAD), postoperative mortality rates for DeBakey type I and II dissections remain high, around 25–30%. Given the life-threatening nature and urgency of this condition in cardiac surgery, a thorough knowledge of the hemodynamics involved is essential. In this context, virtual modeling of ascending aorta resection and tube graft implantation enables accurate visualization of blood flow and pressure distribution in the surgically treated aorta, eliminating the need for direct physical intervention.

The finite element method has been extensively applied to investigate blood flow and related hemodynamic parameters in the aorta and its branches. Previous studies have used this approach to analyze physiological conditions in healthy aortas (Shahcheranhi, 2002; Wen, 2010), pathological alterations in dissected aortas (Karmonik, 2011; Tang, 2012; Karmonik, 2012), as well as aneurysmal changes (Borghi, 2008; Tan, 2009; Filipovic, 2013b). Collectively, these computational approaches have proven to be crucial for advancing the understanding of vascular pathologies and for supporting both diagnostic assessment and treatment planningBuilding on the importance of precise diagnostics and personalized treatment, recent research has focused on patient-specific modeling for type B aortic dissection, a severe condition requiring accurate simulations for effective management (Armour et al. 2022). Using advanced computational techniques and CT imaging, researchers developed individualized models that reflect unique patient anatomy and physiology. Model validation was essential, comparing predictions with clinical outcomes to ensure reliability. Findings demonstrated that these models improve the understanding of hemodynamics, aid in predicting disease progression, and guide surgical decisions. Despite challenges such as anatomical variability, computational modeling enhances clinical decision-making, with future research aiming to expand datasets to improve applicability in personalized medicine.

Recent studies have also examined the impact of aortic wall elasticity on blood flow dynamics in patients who underwent surgical repair of type A aortic dissection (Zhu et al., 2022). Using computed tomography angiography data, fluid–structure interaction simulations were developed to provide a comprehensive assessment of post-surgical hemodynamics. The findings demonstrated that wall elasticity played a key role in shaping flow characteristics: more compliant wall models were associated with reduced blood velocity and wall shear stress compared to rigid models. Importantly, regions of low shear stress expanded in flexible wall simulations, indicating a potentially greater risk of thrombus development. By contrast, the pressure differences between the true and false lumens were minimal - 0.25 mmHg and 0.2 mmHg for two cases - suggesting that rigid-wall assumptions may still be adequate for pressure estimation. Furthermore, turbulence appeared more pronounced under flexible conditions, reflecting increased flow disturbances. Adjusting the Young’s modulus of the aortic wall further

decreased both velocity and shear stress, emphasizing the necessity of accounting for wall elasticity in computational models to improve predictions of surgical outcomes.

The role of computational modeling extends beyond aortic dissection to other vascular conditions, such as ascending thoracic aortic aneurysms (ATAA), which can lead to dissections even below the 55 mm surgical threshold (Valente et al. 2022). Researchers constructed a patient-specific computational framework in SimVascular, employing fluid–structure interaction simulations to investigate the biomechanics of ATAA and provide guidance for clinical decision-making. Constructed from CT scans, the model accurately represented aortic geometry, enhancing simulation precision. The study highlighted how hemodynamic and biomechanical analyses improve the understanding of ATAA progression and rupture risk. Optimization of mesh generation in SimVascular further enhanced computational efficiency without compromising accuracy, making the approach more viable for clinical use. The study tracked velocity, pressure, and wall shear stress across the cardiac cycle, revealing significant pressure variations in ATAA, which are crucial for assessing wall stress and potential rupture. The authors emphasized the need for model validation with in vivo data, such as 4D MRI, to improve reliability and refine predictions for aneurysm behavior and treatment planning.

Aortic dissection remains a significant medical challenge, particularly after surgical intervention, necessitating a deeper understanding of post-operative blood flow dynamics to anticipate complications (Wang et al. 2022). Advanced computational fluid dynamics simulations were employed to analyze these complex hemodynamic processes in post-operative patients. To ensure accuracy, high-resolution imaging techniques - including computed tomography and four-dimensional flow magnetic resonance imaging - were integrated into the modeling process. The resulting patient-specific models provided valuable insights into individual blood flow conditions, aiding in the prediction of post-surgical complications. By analyzing flow patterns and pressure distributions within the aorta, the study identified regions at risk for further dissection or rupture, which is critical for patient safety. Findings suggested that certain surgical techniques yield more favorable hemodynamic outcomes, underscoring the potential benefits of personalized surgical planning. Additionally, the study examined the impact of varying boundary conditions, revealing how differences in blood flow dynamics influence aortic stability after surgery. he results add to the expanding evidence supporting personalized treatment strategies in cardiovascular surgery, highlighting the value of integrating computational modeling into clinical practice for improved decision-making in complex scenarios.

While numerous studies have explored the causes of specific types of aortic dissection and their underlying mechanisms, few have investigated the fate of the false lumen after surgery or how the procedure resolves malperfusion issues and blood flow obstructions in aortic branches. This study aims to fill that gap by using numerical simulations to analyze pressure, shear stress, and velocity in preoperative models of both the true and false lumens, providing a clearer understanding of their interactions. Following this, virtual surgical interventions were performed to generate postoperative models based on physician recommendations, and numerical analyses were conducted. These findings offer a comprehensive view of how surgical interventions alter hemodynamic conditions, contributing to more informed clinical strategies for treating aortic dissection.

3. Fundamental relations

A fluid is defined as a substance that undergoes continuous deformation when subjected to tangential forces. While gases are compressible - meaning their volume varies with changes in

pressure - liquids are generally treated as incompressible, since a fixed quantity of liquid maintains its volume under pressure variations. This behavior arises from intermolecular interactions: the attractive forces between liquid molecules are sufficient to resist significant volume change, but still weaker compared to solids, which allows for deformation.

The continuity equation provides the mathematical expression of the law of mass conservation. This principle can be applied to both an infinitesimal fluid element of mass dm and a finite fluid mass m. In a continuous flow field, the mass of a fluid particle remains constant during its motion. By applying Reynolds' transport theorem to the law of mass conservation, the following relation for an arbitrary control volume V can be derived (Filipović, 1999):

$$\frac{D}{Dt}\int_V (f\rho)dV = \int_V \left(\frac{\partial f}{\partial t} + v_i \frac{\partial f}{\partial x_i}\right)\rho dV = \int_V \rho \frac{Df}{Dt} dV \tag{1}$$

The Navier–Stokes equations govern the behavior of viscous, incompressible fluids. They constitute a set of partial differential equations derived directly from Newton's second law of motion. For a given fluid volume at time t, external influences can be expressed as surface forces fS acting per unit area and body forces fB acting per unit mass. Based on the momentum conservation principle, the following relation can be established:

$$\frac{D}{Dt}\int_V \rho v dV = \int_V \mathbf{b} dV + \int_S \mathbf{p} dS \tag{2}$$

By applying equation (1), which represents the mass conservation equation, the previous equation reduces to the following form:

$$\int_V \rho \frac{D\mathbf{v}}{Dt} dV = \int_V \mathbf{f}^B dV + \int_S \mathbf{f}^S dS \tag{3}$$

Viscous incompressible fluid motion is governed by the Navier–Stokes equations, a set of partial differential equations originating from Newton's second law. Considering a fluid volume at time t, with surface forces fS (per unit area) and body forces fB (per unit mass), the momentum balance leads to the following expression:

$$\rho\left(\frac{\partial v_i}{\partial t} + v_j \frac{\partial v_i}{\partial x_j}\right) = -\frac{\partial p}{\partial x_i} + \mu\left(\frac{\partial^2 v_i}{\partial x_j \partial x_j} + \frac{\partial^2 v_j}{\partial x_j \partial x_i}\right) + f_i^B \tag{4}$$

4. Methods

4.1 Geometry

The 3D aorta models were generated from a series of slices acquired in vivo using CT spiral imaging (Institute of Cardiovascular Diseases, Sremska Kamenica). Various thresholding and flood-fill segmentation techniques were employed to create multiple masks for selecting the dissected aorta and its primary branches. For this study, geometric data from two patients were used, with a scan resolution of 0.7 mm/pixel. Smoothing processes were applied to eliminate pixelation artifacts, while dilation was used to compensate for any volume reduction caused by smoothing. A total of two preoperative and two postoperative aortic dissection geometries were reconstructed, with the postoperative models created according to physicians' recommendations through computer manipulation.

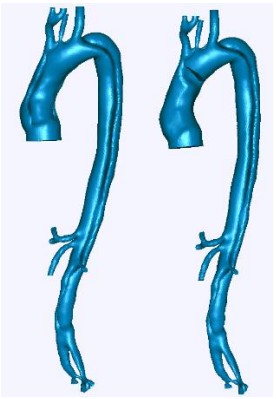

a) b)

Fig. 2. 3D model of dissected aorta. (a) before surgery; (b) after virtual surgery

For the patient shown in Fig. 2b, the postoperative model demonstrated closure of the false lumen, while the ascending aorta was reconstructed using a simulated tube graft.

4.2 Computational fluid dynamics

In this study, blood was treated as an incompressible, Newtonian fluid with a density of 1056 kg/m³ and a dynamic viscosity of 3.5 mPa·s. Considering the high shear rates typically present in large arteries, the Newtonian fluid assumption is justified (Karmonik 2012). The flow was assumed to be laminar, with an average aortic blood flow rate of 5 L/min. Mean blood velocity for each patient was determined based on vessel diameter and flow rate data. A physiological velocity waveform was applied at the inlet.

According to the literature, fluid-structure interactions in the aorta are commonly modeled using hyperelastic, homogeneous, and isotropic materials, with elastic modulus values ranging from 0.4 MPa (Reymond 2013; Colciago 2014) up to 3 MPa (Nathan 2011). In this study, an elastic modulus of 2.5 MPa and a Poisson's ratio of 0.45 were used. The simulations were performed using eight-node finite elements and the PAKSF solver (Filipovic 1999). A parabolic velocity profile was applied at the ascending aorta inlet, with a zero-pressure boundary condition at the outlet (Karmonik 2011). The simulations encompassed a complete cardiac cycle, with results reported at peak systole (0.22s).

4. Results

4.1 Preoperative models

The numerical analysis of the interaction between the true and false lumens focuses on determining key hemodynamic parameters, including shear stress, pressure distribution, and flow velocities. Fig. 3 illustrates the aortic anatomy and highlights the specific segments where the dissection analysis is performed (Erbel 2014). These marked segments, referenced from the literature, represent critical locations where significant changes in aortic diameter occur.

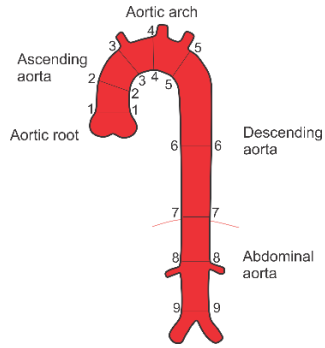

Fig. 3. Aortic anatomy and observed sections

Patient #01 was a 60-year-old male, non-smoker, diagnosed with hypotension and an acute DeBakey type I aortic dissection. The entry tear measured 4.25 cm² and was situated 81 mm from the apex of the aortic arch. A re-entry tear, with an area of 8.77 cm², was located 9.1 mm from the aortic bifurcation. The true lumen volume was measured at 389.64 cm³, while the false lumen volume was 133.83 cm³. Table 1 provides the precise ratios of the relevant cross-sectional areas along the aorta. It is noteworthy that, in the mid-aortic arch (section 4-4) and the proximal descending aorta (section 5-5), the false lumen area exceeds that of the true lumen when comparing cross-sectional measurements.

	Cross-sectional area [cm2]			*Cross-sectional area [%]*	
Section	Total area	True lumen	False lumen	True lumen	False lumen
1-1	21.59	21.59	/	100.00	/
2-2	17.77	14.30	3.47	80.46	19.54
3-3	13.62	9.81	3.80	72.04	27.96
4-4	10.51	4.44	6.07	42.25	57.75
5-5	9.52	3.90	5.61	41.06	58.94
6-6	7.08	5.26	1.82	74.26	25.74
7-7	8.00	7.08	0.92	88.43	11.57
8-8	4.89	3.83	1.06	78.23	21.77
9-9	4.31	3.45	0.86	79.95	20.05

Table 1. Patient #01 – Cross-sectional area of true and false lumen

Figure 4 presents the distributions of shear stress, pressure, and velocity. The results indicate that, starting from the ascending aorta, the false lumen maintains a higher pressure up to the level of the diaphragm, marking the end of the thoracic aorta. Within the ascending aorta, the shear stress in the false lumen reaches up to 7.42 Pa. The highest shear stress values were recorded at the brachiocephalic trunk and along the left common subclavian artery, both measuring 20.50 Pa. Since the response of dissected regions to shear stress is not yet fully understood, it is plausible to assume that their behavior resembles that of aneurysms (Shojima 2004). Furthermore, previous studies (Kondo 1997; Filipovic 2013a) have demonstrated a correlation between elevated shear stress and the expansion of tears, formation of additional

tears, and development of aneurysms. Through the brachiocephalic artery, which was associated with the right lumen, a flow rate of 15.77 cm³/s was observed, accounting for 18.79% of the total flow.

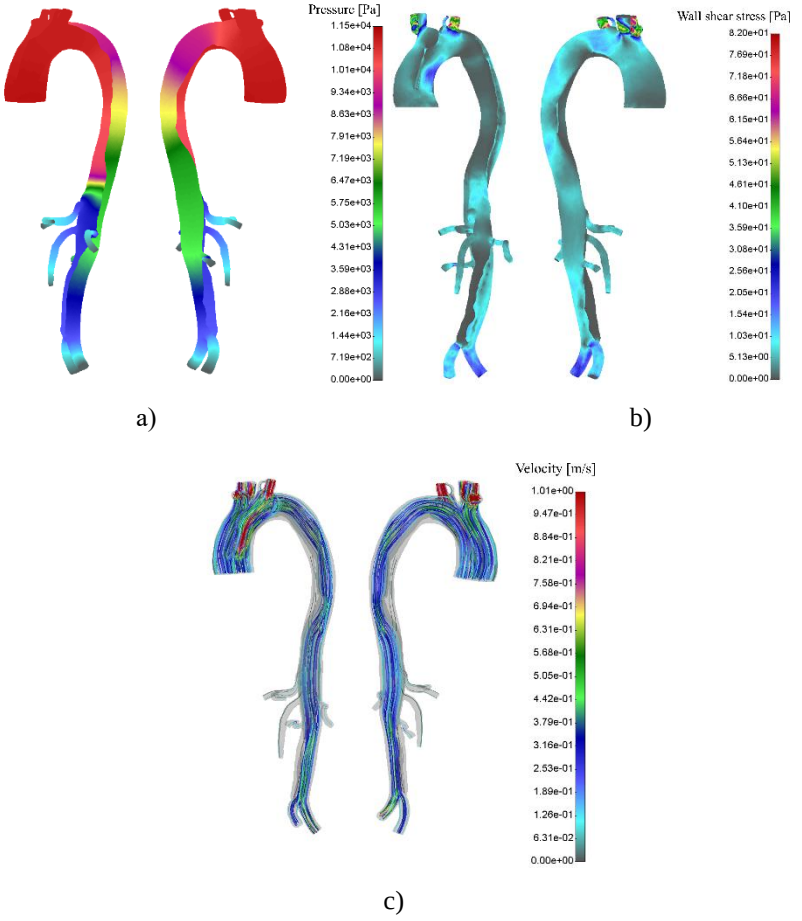

Fig. 4. Results of numerical analysis of the preoperative model of patient #01: a) pressure, b) wall shear stress, c) velocity streamlines

The false lumen, which receives 35.43% of the total blood flow, has become the primary supply route for the left common carotid artery, delivering 2.61 cm³/s (3.12% of total flow). The flow through the left subclavian artery is 9.22 cm³/s (10.98%). Additionally, the celiac branch and the superior mesenteric artery, with flow rates of 10.27 cm³/s (12.31%) and 7.81 cm³/s (9.29%) respectively, are also supplied by the false lumen. The left renal artery is subject to static obstruction, receiving blood from both the true and false lumens. In the left renal branch, blood velocity is 0.16 m/s, resulting in a flow rate of 7.58 cm³/s (9.03%), while the right renal branch, supplied solely by the right lumen, has a flow rate of 8.41 cm³/s (10.02%). Both iliac branches originate from the right lumen, with the right and left iliac arteries carrying 10.61 cm³/s (12.62%) and 11.62 cm³/s (13.84%) of the flow, respectively.

Patient #02 is a 51-year-old, morbidly obese male, smoker, diagnosed with hypertension, diabetes, hyperlipidemia, and acute DeBakey type I aortic dissection. The entry tear measures 10.16 cm² and is located 95 mm from the apex of the aortic arch. The true lumen has a volume of 36.06 cm³, while the false lumen measures 102.32 cm³. As indicated in the following table, the false lumen demonstrates significantly higher values - nearly four times greater - in the mid-descending aorta and the diaphragmatic region.

	Cross-sectional area [cm²]			*Cross-sectional area [%]*	
Section	Total area	True lumen	False lumen	True lumen	False lumen
1-1	32.07	32.07	0.00	100.00	0.00
2-2	15.82	11.79	4.03	74.52	25.48
3-3	8.60	6.93	1.66	80.64	19.36
4-4	6.47	3.79	2.68	58.56	41.44
5-5	5.64	3.55	2.09	63.00	37.00
6-6	5.79	1.34	4.45	23.15	76.85
7-7	4.72	0.96	3.76	20.41	79.59
8-8	3.04	3.04	0.00	100.00	0.00
9-9	2.98	2.98	0.00	100.00	0.00

Table 2. Patient #02 – Cross-sectional area of true and false lumen

Figure 5 presents the simulation results for Patient #02. The results show that the pressure values in the true and false lumens remain similar up to the mid-thoracic aorta. Similar to the previous patient, the false lumen exhibits very high shear stress in the ascending aorta, reaching up to 29.33 Pa. Elevated shear stress is also observed at the origins of the brachiocephalic artery and the left common carotid artery. As previously noted, such high shear stress levels can negatively impact endothelial function.

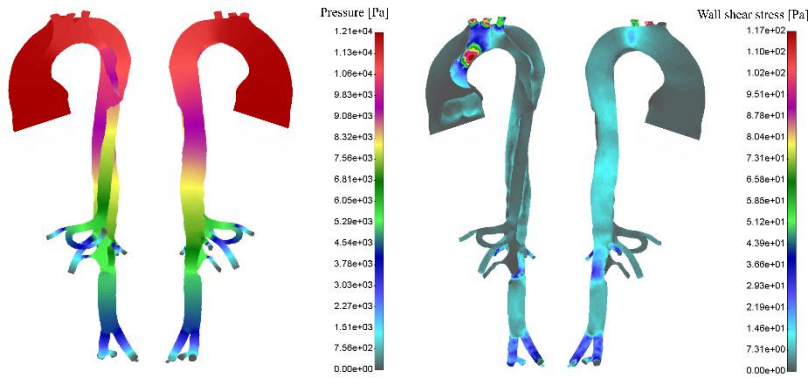

a) b)

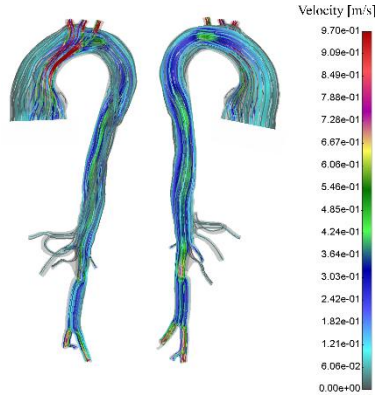

c)

Fig. 5. Results of numerical analysis of the preoperative model of patient #02: a) pressure, b) wall shear stress, c) velocity streamlines

The false lumen accounted for 41.18% of the total blood flow. All branches of the aortic arch were supplied entirely by the false lumen, with flow rates of 12.52 cm³/s (14.91%) through the brachiocephalic artery, 9.64 cm³/s (11.48%) through the left carotid artery, and 8.45 cm³/s (10.06%) through the left subclavian artery. The celiac artery, also originating from the false lumen, received a flow of 8.31 cm³/s (9.18%), while the superior mesenteric artery had a flow of 6.81 cm³/s (8.11%). The right renal artery, which is connected to the true lumen, carried a flow of 7.01 cm³/s (8.34%). An interesting observation was made regarding the left renal artery: it received part of its supply from the true lumen (6.81 cm³/s, 8.12%) and part from the false lumen (1.97 cm³/s, 2.35%). Both iliac arteries branched from the true lumen, with the right iliac artery carrying 12.13 cm³/s (14.44%) and the left iliac artery 10.85 cm³/s (12.93%).

4.2 Postoperative models

Postoperative mortality remains high among patients, largely due to limited understanding of how surgical procedures influence blood flow within the aorta and its branches. Computational simulations of preoperative models enable the generation of virtual postoperative geometries for individual patients, providing clinicians with valuable insight into the potential outcomes of specific surgical interventions (Filipovic 2015). An additional benefit of this approach is the ability to evaluate various surgical techniques through multiple models, allowing for a more thorough analysis of different scenarios.

In the postoperative geometry model for Patient #01, the ascending aorta was replaced with a stent graft, and the false lumen was sealed. After surgery, pressure within the true lumen increased, while pressure in the false lumen decreased. The maximum pressure recorded in the true lumen of the ascending aorta reached 15,812 Pa (Fig. 6a). Blood flow through the brachiocephalic artery rose from 15.77 cm³/s to 19.39 cm³/s. Flow through the left common carotid artery decreased from 2.61 cm³/s to 0.74 cm³/s, and flow through the left subclavian artery was reduced by 78.63% to 1.97 cm³/s. The celiac artery flow dropped by 30.18% to 7.17 cm³/s, while the superior mesenteric artery flow decreased by 46.02% to 4.21 cm³/s.

In contrast, the flow in the left renal artery increased by 34.3% to 10.18 cm³/s, and the right renal artery flow rose from 8.41 cm³/s to 11.30 cm³/s. The iliac arteries also exhibited increased flow: the right iliac artery flow rose by 33.3% to 14.13 cm³/s, and the left iliac artery flow increased by 26.67% to 14.72 cm³/s.

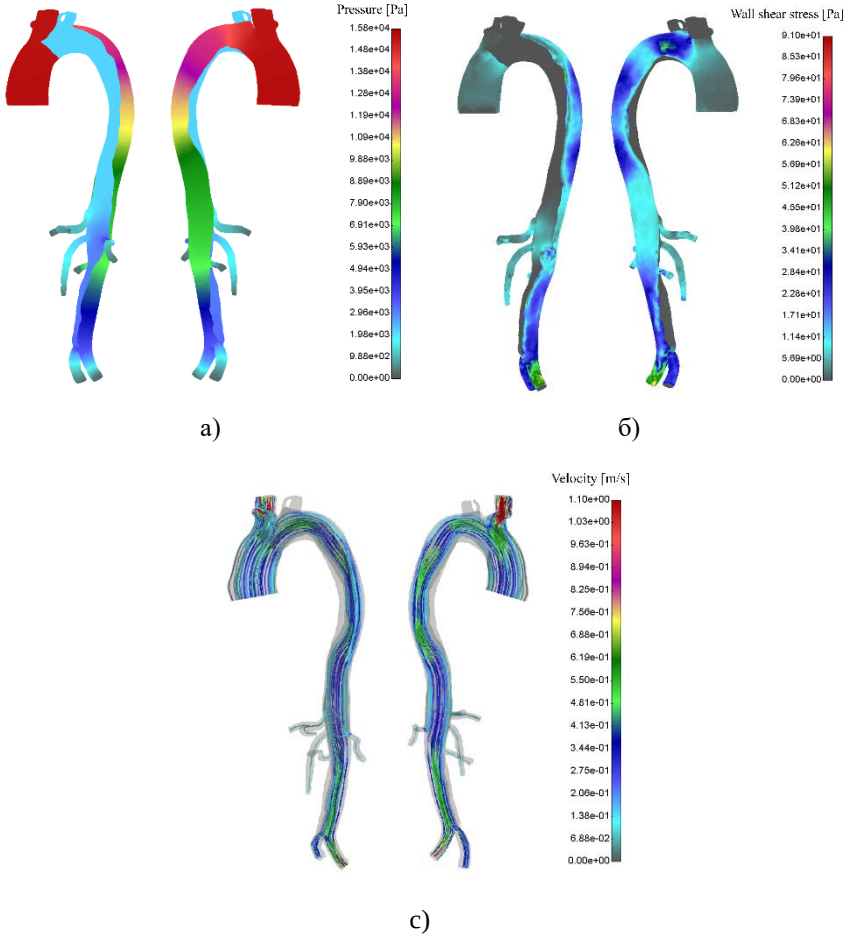

а) б)

c)

Fig. 6. Results of numerical analysis of the postoperative model of patient #01: a) pressure, b) wall shear stress, c) velocity streamlines

The suggested postoperative approach, which entails replacing the ascending aorta and simultaneously sealing the false lumen, generally leads to favorable surgical outcomes. Although a reduction in flow is observed in the left subclavian and left common carotid arteries, the majority of other branches experience increased flow. Virtual manipulation of Patient #01's preoperative model offers a more detailed understanding of blood flow distribution within the aortic arch and its distal branches. This technique enables clinicians to anticipate whether postoperative perfusion will be adequate to meet the metabolic demands of the body's organs.

For Patient #02, the postoperative model also involved replacing the ascending aorta with a stent graft and eliminating flow through the false lumen. However, because the aortic arch branches were initially supplied by the false lumen, it was necessary to redirect all three branches to the true lumen and evaluate the resulting changes in blood flow dynamics.

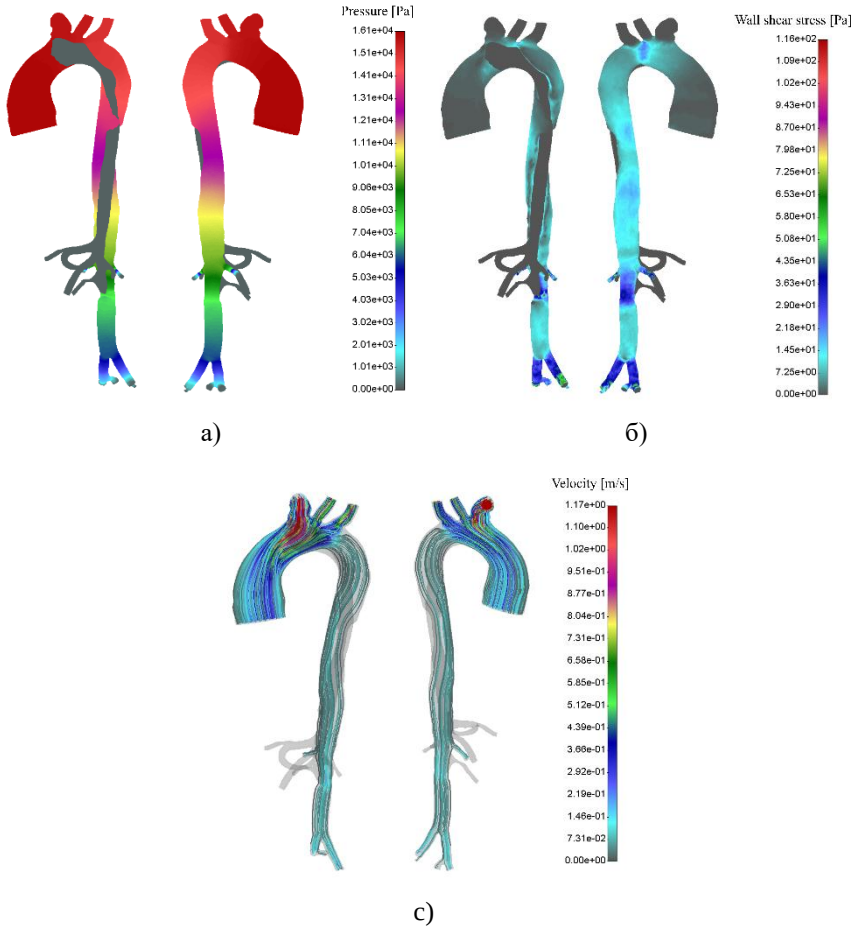

Fig. 7. Results of numerical analysis of the postoperative model of patient #02: a) pressure, b) wall shear stress, c) velocity streamlines

Figure 7 illustrates the redistribution of pressure, showing that the true lumen once again exhibits higher values, increasing from 12,140 Pa to 16,106 Pa. Blood flow through the aortic arch branches is as follows: 14.14 cm³/s through the brachiocephalic artery (a 12.93% increase), 10.71 cm³/s through the left carotid artery (an 11.09% increase), and 10.14 cm³/s through the left subclavian artery (a 20% increase). However, after the procedure, the celiac trunk, superior mesenteric artery, and right renal artery receive no flow due to the absence of a re-entry tear in the reconstructed segment of the aorta. In a real clinical scenario, minimal flow might be present in these branches due to the closed circulatory system, but such a surgical outcome would still fall short of expectations.

The left renal artery, now supplied by the true lumen, sees its flow increase from 6.81 cm³/s to 10.65 cm³/s (a 56.38% rise). The iliac arteries also show increased flow postoperatively, with the right iliac artery at 14.88 cm³/s (up 22.67%) and the left at 12.71 cm³/s (up 17.14%).

In summary, while the postoperative procedure partially achieves its objectives—improving flow through the branches of the aortic arch and thus supporting upper body function—the lack of a re-entry tear in the reconstructed aorta results in inadequate flow to

branches of the abdominal aorta, potentially compromising kidney function. This limitation helps explain the persistently high mortality rate following surgery (Suzuki 2003).

4. Conclusions

Cardiovascular diseases remain the leading cause of death in all developed countries, and our country is classified among those with a high risk of mortality from these conditions. In this study, three-dimensional simulations were performed to analyze the hemodynamic behavior of blood in aortas affected by acute dissection. DICOM images from two patients, obtained from the Institute for Cardiovascular Diseases of Vojvodina, were reconstructed into 3D geometries for detailed examination.

The primary objective of these simulations was to numerically assess the relationship between the true and false lumens in cases of acute aortic dissection. Accurately predicting how the false lumen will behave and progress is essential for effective clinical decision-making and treatment planning. The preoperative model simulations provided numerical data on pressure, shear stress, and blood flow velocities throughout the dissected segments of the aorta and its reconstructed branches. Each patient's aorta was divided into nine segments, allowing for measurement of total cross-sectional areas for the entire vessel, as well as for the true and false lumens individually.

The postoperative model simulations involved numerical analyses based on surgical procedures recommended by physicians. This method underscored the value of virtual surgeries, which make it possible to anticipate the effects of an operation on future organ function. Accurate determination of parameters such as pressure, shear stress, and especially flow velocity enables more reliable assessments of postoperative recovery and minimizes errors in preoperative assumptions.

The findings from this study suggest that numerical simulations and virtual surgical planning are extremely useful in clinical practice, particularly for managing complex vascular conditions like aortic dissection. These techniques not only support personalized treatment strategies but also enhance clinical decision-making by providing precise, data-driven insights, ultimately reducing complication risks and improving outcomes. As cardiovascular diseases continue to pose significant challenges, adopting such innovative approaches in clinical settings represents an important step forward in improving patient care and quality of life.

Acknowledgements: This research is funded by the Serbian Ministry of Education, Science, and Technological Development [451-03-136/2025-03/200378 (Institute for Information Technologies, University of Kragujevac).

References

Armour C H, Guo B, Saitta S, Saitta S, Pirola S, Liu Y, Dong Z, Xu X Y (2022). Evaluation and verification of patient-specific modelling of type B aortic dissection. *Computers in Biology and Medicine*, *140*, 105053. https://doi.org/10.1016/J.COMPBIOMED.2021.105053**.**

Augoustides J G T, Andritsos M (2010). Innovations in aortic disease: the ascending aorta and aortic arch, *J Cardiothorac Vasc Anesth*, 24, 198-207.

Borghi A, Wood N B, Mohiaddin R H, Xu X Y (2008). Fluid-solid interaction simulation of flow and stress pattern in thoracoabdominal aneurysms: a patient-specific study, *Journal of Fluids and Structures*, 24(2), 270-280.

Colciago C M, Deparis S, Quarteroni A (2014). Comparisons between reducedorder models and full 3D models for fluid-structure interaction problemsin haemodynamics, *Journal of Computational and Applied Mathematics*, 265, 120-138.

Culliford A T, Ayvaliotis B, Shemin R, Colvin S B, Isom O W, Spencer F C (1982). Aneurysms of the ascending aorta and transverse arch: surgical experience in 80 patients, *J Thorac Cardiovasc Surg*, 82, 701-710.

Elefteriades J A, Lovoulos C J, Coady M A, Tellides G, Kopf G S, Rizzo J A (1999). Management of descending aortic dissection, *Ann Thorac Surg*, 67, 2002-2005.

Erbel R, Aboyans V, Boileau C, Bossone E, Bartolomeo R D, Eggebrecht H, Evangelista A, Falk V, Frank H, Gaemperli O, Grabenwöger M, Haverich A, Iung B, Manolis A J, Meijboom F, Nienaber C A, Roffi M, Rousseau H, Sechtem U, Sirnes P A, Allmen R S, Vrints C J (2014) ESC Guidelines on the diagnosis and treatment of aortic diseases: Document covering acute and chronic aortic diseases of the thoracic and abdominal aorta of the adult. The Task Force for the Diagnosis and Treatment of Aortic Diseases of the European Society of Cardiology (ESC), *Eur Heart J*, 35(41), 2873-2926.

Filipovic N (1999). Numerical Analysis of Coupled Problems: Deformable Body and Fluid Flow. Ph.D. Thesis, Faculty of Mech. Engrg., University of Kragujevac, Serbia.

Filipovic N, Nikolic D, Saveljic I, Djukic T, Adjic O, Kovacevic P, Cemerlic-Adjic N, Velicki L (2013b). Computer simulation of thromboexclusion of the complete aorta in the treatment of chronic type B aneurysm, *Computer Aided Surgery*, 18(1-2), 1-9.

Filipovic N, Saveljic I, Nikolic D, Milosevic Z, Kovacevic P, Velicki L (2015). Numerical simulation of blood flow and plaque progression in carotid–carotid bypass patient specific case, *Computer Aided Surgery*, 20(1), 1-6.

Filipovic N, Teng Z, Radovic M, Saveljic I, Fotiadis D, Parodi O (2013a). Computer simulation of three dimensional plaque formation and progression in the carotid artery, *Medical & Biological Engineering & Computing*, 51(6), 607-616.

Golledge J, Eagle K A (2008). Acute aortic dissection, *TheLancet*, 372(9632), 55-66.

Hagan P G, Nienaber C A, Isselbacher E M, Bruckman D, Karavite D, Russman P (2000). The International Registry of Acute Aortic Dissection(IRAD): new insights into an old disease, *JAMA*, 283, 897-903.

Karmonik C, Bismuth J, Davies M G, Shah D J, Younes H K, Lumsden A B (2011). A computational fluid dynamics study pre-and post-stent graft placement in an acute type B aortic dissection, *Vascular and Endovascular Surgery*, 45(2), 157-164.

Karmonik C, Partovi S, M¨uller-Eschner M (2012). Longitudinal computational fluid dynamics study of aneurysmal dilatation in a chronic DeBakey type III aortic dissection, *Journal of Vascular Surgery*, 56(1), 260-263.

Khan I A, Nair C K (2002). Clinical, diagnostic, and management perspectivesof aortic dissection, *Chest*, 122, 311-328.

Kojić M, Slavković R, Živković M, Grujović N (1998). Metod Konačnih Elemenata I, Mašinski fakultet u Kragujevcu.

Kondo S, Hashimoto N, Kikuchi H, Hazama F, Nagata I, Kataoka H (1997). Cerebral aneurysms arising at nonbranching sites. An experimental study, *Stroke*, 28, 398-403.

Miller D C (1991). Surgical management of acute aortic dissection: new data, *Semin Thorac Cardiovasc Surg*, 3, 225-237.

Nathan D P, Xu C, Gorman J H, Fairman R M, Bavaria J E,Gorman R C, Chandran K B, Jackson B M (2011). Pathogenesisof acute aortic dissection: a finite element stress analysis, *The Annals ofThoracic Surgery*, 91(2), 458-463.

Reymond P, Crosetto P, Deparis S, Quarteroni A, Stergiopulos N (2013). Physiological simulation of blood flow in the aorta: Comparison of hemodynamicindices as predicted by 3-D FSI, 3-D rigid wall and 1-D models, *Medical Engineering and Physics*, 35(6), 784-791.

Shahcheranhi N, Dwyer H A, Cheer A Y, Barakat A I, Rutaganira T (2002). Unsteady and three-dimensional simulation of blood flow in the human aortic arch, *Journal of Biomechanical Engineering*, 124(4), 378-387.

Shojima M (2004). Magnitude and Role of Wall Shear Stress on CerebralAneurysm: Computational Fluid Dynamic Study of 20 Middle CerebralArtery Aneurysms, *Stroke*, 35(11), 2500-2505.

Suzuki T, Mehta R H, Ince H, Nagai R, Sakomura Y, Weber F, Suniyoshi T, Bossone E, Trimarchi S, Cooper J V, Smith D E, Isselbacher E M, Eagle K A, Nienaber C A (2003). Clinical profiles and outcomes of acute type B aortic dissection in the current era: lessons learned from the International Registry of Aortic Dissection (IRAD), *Circulation*, 108, 312-317.

Svensson L G, Kouchoukos N T, Miller D C (2008). Expert consensus document on the treatment of descending thoracic aortic disease using endovascular stent-grafts, *Ann Thorac Surg*, 85, 1-41.

Tan F P P , Borghi A , Mohiaddin R H, Wood N B, Thom S, Xu X Y (2009). Analysis of flow patterns in a patient-specific thoracic aortic aneurysm model, *Computers and Structures*, 87(11-12), 680-690.

Tang A Y S, Fan Y, Cheng S W K, Chow K W (2012). Biomechanical factors influencing type B thoracic aortic dissection: computational fluid dynamics study, *Engineering Applications of Computational Fluid Mechanics*, 6, 622-632.

Trimarchi S, Nienaber C A, Rampoldi V (2006). Role and results of surgery in acute type B aortic dissection: insights from the International Registry of Acute Aortic Dissection (IRAD), *Circulation*, 114, 357-364.

Valente R B, Mourato A, Brito M, Xavier J F P, Tomás A C, Avril S (2022). Fluid–Structure Interaction Modeling of Ascending Thoracic Aortic Aneurysms in SimVascular, *Biomechanics*, 2(2), 189-204.

Wang Q L, Guo X W, Stäb D, Jin N, Poon E K W, Lim R P, Ooi A (2022). Computational fluid dynamic simulations informed by CT and 4D flow MRI for post-surgery aortic dissection – A case study, *International Journal of Heat and Fluid Flow*, 96, 108986. https://doi.org/10.1016/j.ijheatfluidflow.2022.108986**.**

Wen C Y, Yang A S, Tseng L Y, Chai J W (2010). Investigation of pulsatile flowfield in healthy thoracic aorta models, *Annals of Biomedical Engineering*, 38(2), 391-402.

Zhu Y, Mirsadraee S, Rosendahl U, Pepper J, Xu X (2022). Fluid-Structure Interaction Simulations of Repaired Type A Aortic Dissection: a Comprehensive Comparison With Rigid Wall Models, *Frontiers in Physiology*, 13. https://doi.org/10.3389/fphys.2022.913457**.**